The Cryosphere
Open Access
Discussions

Ocean properties, ice–ocean interactions, and calving front morphology at two major west Greenland glaciers

N. Chauché[1], A. Hubbard[1], J.-C. Gascard[2], J. E. Box[3,4], R. Bates[5], M. Koppes[6], A. Sole[7], and H. Patton[1]

[1]Department of Geography and Earth Science, Aberystwyth University, UK
[2]Laboratoroire d'Océanographie et du Climat, Expérimentation et approche Numérique, Université Pierre et Marie Curie, France
[3]Byrd Polar Research Center, The Ohio State University, Columbus, Ohio, USA
[4]Geological Survey of Denmark and Greenland, Copenhagen, Denmark
[5]School of Geography and Geosciences, St-Andrews University, UK
[6]Department of Geography, University of British Columbia, CA, USA
[7]Department of Geography, University of Sheffield, UK

Correspondence to: N. Chauché (noc3@aber.ac.uk)

TCD

7, 5579–5611, 2013

Ice-ocean interaction at two major west Greenland glaciers

N. Chauché et al.

Title Page	
Abstract	Introduction
Conclusions	References
Tables	Figures

|◄ | ►|

◄ | ►

Back | Close

Full Screen / Esc

Printer-friendly Version

Interactive Discussion

Abstract

Warm sub-polar mode water (SPMW) has been identified as a primary driver of mass loss of marine terminating glaciers draining the Greenland Ice Sheet (GrIS) yet, the specific mechanisms by which SPMW interacts with these tidewater termini remain uncertain. We present oceanographic data from Rink Glacier (RG) and Store Glacier (SG) fjords, two major marine outlets draining the western sector of the GrIS into Baffin Bay over the contrasting melt-seasons of 2009 and 2010. Submarine melting occurs wherever ice is in direct contact with warmer water and the consistent presence of $2.8\,^{\circ}\mathrm{C}$ SPMW adjacent to both ice fronts below 400 m throughout all surveys indicates that melting is maintained by a combination of molecular diffusion and large scale, weak convection, diffusional (hereafter called ubiquitous) melting. At shallower depths (50–200 m), cold, brine-enriched water (BEW) formed over winter appears to persist into the summer thereby buffering this melt by thermal insulation. Our surveys reveal four main modes of glacier–ocean interaction, governed by water depth and the rate of glacier runoff water (GRW) injected into the fjord. Deeper than 200 m, submarine melt is the only process observed, regardless of the intensity of GRW or the depth of injection. However, between the surface and 200 m depth, three further distinct modes are observed governed by the GRW discharge. When GRW is weak ($\lesssim 1000\,\mathrm{m^3\,s^{-1}}$), upward motion of the water adjacent to the glacier front is subdued, weak forced or free convection plus diffusional submarine melting dominates at depth, and seaward outflow of melt water occurs from the glacier toe to the base of the insulating BEW. During medium intensity GRW ($\sim 1500\,\mathrm{m^3\,s^{-1}}$), mixing with SPMW yields deep mixed runoff water (DMRW), which rises as a buoyant plume and intensifies local submarine melting (enhanced buoyancy-driven melting). In this case, DMRW typically attains hydrostatic equilibrium and flows seaward at an intermediate depth of ~ 50–150 m, taking the BEW with it. Strong GRW ($\gtrsim 2000\,\mathrm{m^3\,s^{-1}}$) yields vigorous, buoyant DMRW, which has sufficient vertical momentum to break the sea surface before sinking and flowing seaward, thereby leaving much of the BEW largely intact. Whilst these modes

of glacier–ocean interaction significantly affect the ice–ocean interaction in the upper water column (0–200 m), below 200 m both RG and SG are dominated by the weak forced convection/diffusional (herein termed ubiquitous) melting due to the presence of SPMW.

1 Introduction and background

The sub-polar gyre of the North Atlantic circulation advects deep (> 400 m depth), warm (> 3 °C) and saline (> 34.8 PSU) water around the coast of Greenland driving a massive and largely undetermined external heat source into this sensitive Arctic environment (Christoffersen et al., 2012; Holland et al., 2008; Mortensen et al., 2011; Straneo et al., 2012). Marine terminating outlet glaciers draining the Greenland ice sheet are connected to this deep water body by over-deepened troughs which provide the opportunity for warm and saline ocean water to directly access their ice fronts, profoundly affecting their energy and mass balance (Hanna et al., 2008; Pfeffer, 2007; Rignot et al., 2010). In West Greenland, a trigger mechanism for the retreat of Jakobshavn Glacier observed since 2001, has been attributed to warming of subsurface water adjacent to the fjord mouth in Disco Bay (Holland et al., 2008). Similarly, warm oceanic waters of sub-tropical origin were identified circulating within Sermilik fjord in East Greenland and have been implicated in the retreat of Helheim Glacier over the last decade (Straneo et al., 2011, 2010). Furthermore, two distinct phases of dynamic ice loss (1985–1990 and 2005–2010) across the Melville Coast in NW Greenland have recently been attributed to oceanic rather than atmospheric forcing (Kjær et al., 2012). An implicit assumption of these studies is that the warm sub-polar oceanic water is in direct contact with and hence undermining large outlet glaciers draining the ice sheet (Holland et al., 2008; Kjær et al., 2012; Motyka et al., 2011; Rignot et al., 2010; Straneo et al., 2012). Despite this assumption, to date few observational studies have focused on the actual ice–ocean interface, in particular on the controls governing subma-

rine melt and the accompanying mass and energy exchanges which determine outlet glacier and fjord dynamics alike.

Several different modes of interaction between fjord water masses and marine terminating ice fronts have been observed, modelled and/or speculated upon, including upwelling caused by subglacial runoff discharge and entrainment of sub-polar mode water (SPMW) (Mugford and Dowdeswell, 2011; Salcedo-Castro et al., 2011; Sole et al., 2012), wind-stress and tide-driven fjord circulation (Straneo et al., 2010; Mortensen et al., 2011; Sole et al., 2012) and submarine melt-driven convection (Jenkins, 1991; Rignot et al., 2010; Sole et al., 2012; Straneo et al., 2010). Circulation in Greenland's deep fjords is more complex than the single convective cell (estuarine circulation) model that has been assumed for the sake of simplicity in previous energy/mass balance calculations (Motyka et al., 2003; Rignot et al., 2010). For instance a vertical superposition of convective cells was observed (Straneo et al., 2011; Sutherland and Straneo, 2012) and more recently modelled (Sciascia et al., 2013; Sole et al., 2012) within two major glacierized fjords of East Greenland. Similarity of glacier–ocean interaction processes as well as Summer–Winter variation for different glacier around Greenland has been found (Straneo et al., 2012). However, no discussion about a potential interannual variation of the relative influence of the interacting processes has been made (Straneo et al., 2012).

In this study, we describe and evaluate the processes driving the interaction of deep SPMW with the ice fronts of two major outlet glaciers draining the western Greenland ice sheet over two successive, contrasting melt-seasons, 2009–2010. Submarine melting and subglacial runoff mixing (causing enhanced buoyancy-driven melting) are identified in association with an additional process, the insulating effect of remnant, cold Brine enriched water (BEW) at shallow depths (50–200 m depth). The spatial and interannual variability of these processes, along with their relative efficacy is controlled by the specific fjord bathymetry, ice-front geometry and glacier meltwater runoff delivery at depth, as well as by the presence of warm and cold ocean water masses advected up to the ice front of each glaciers.

Ice-ocean interaction at two major west Greenland glaciers

N. Chauché et al.

Title Page

Abstract	Introduction
Conclusions	References
Tables	Figures

|◄ | ►|

| ◄ | ► |

| Back | Close |

Full Screen / Esc

Printer-friendly Version

Interactive Discussion

2 Field site

Uummannaq Bay is the only fjord system on the west coast of Greenland that is dominated by an over-deepened trough of $\sim 450\,m$ depth, over $200\,km$ long and $20\,km$ wide that crosses the continental shelf, which provides a direct route for SPMW from Baffin Bay to enter the inner fjord basins and potentially access up to a dozen marine-terminating outlet glaciers (Fig. 1). Identification of cold BEW present in the western sector of Baffin Bay (Melling et al., 2001) suggests that this water body may also be advected into Uummannaq Bay along with SPMW. Local formation of sea ice within the fjord in winter will further contribute to the presence of BEW. The existence of two large marine-terminating outlet glaciers within Uummannnaq bay provides an ideal laboratory to isolate and compare individual glacier responses, with contrasting fjord and ice front geometries and glacier controls, to similar atmospheric and oceanic forcing. Rink Glacier (RG) and Store Glacier (SG) are the second and third most productive outlet glaciers in West Greenland, with calving rates of $16 \pm 2\,km^3\,yr^{-1}$ and $14 \pm 3\,km^3\,yr^{-1}$, respectively (Weidick and Bennike, 2007). This corresponds to 8 % and 7 %, of the total annual discharge for the western Greenland ice sheet (Rignot et al., 2008). Both fjords are wide (5 km) and deep ($> 800\,m$), allowing deep SPMW to penetrate and interact with their respective ice fronts. The maximum water depth at the terminus of RG is 750 m whilst at SG it is 500 m, according to the maximal water depth observed within $\sim 200\,m$ meters of each ice front. Catchment size for RG and SG are $45\,000\,km^2$ and $34\,000\,km^2$ respectively (Rignot et al., 2008) yet, due to its hypsometry, SG has a larger ablation area and hence a greater bulk meltwater runoff contribution compared to its larger neighbour RG.

Title Page

Abstract | Introduction

Conclusions | References

Tables | Figures

|◄ | ►|

◄ | ►

Back | Close

Full Screen / Esc

Printer-friendly Version

Interactive Discussion

3 Methods

3.1 Data collection

Two oceanographic surveys were conducted between 10–22 August 2009 and 5–15 August 2010. These surveys comprised 5 and 7 instrument casts in Rink fjord (RF) and 12 and 11 casts in Store fjord (SF), in 2009 and 2010 respectively. The casts were taken along and across each fjord, at distance between 200 m and 20 km from the glacier front (Figs. 1 and 2) and down to a maximum depth of 750 m. The instrument used was a MIDAS Valeport 2000 Conductivity-Temperature-Depth (CTD) profiler, equipped with a Seapoint turbidity sensor and current profiler (Table 1). Measurements were logged at a sampling rate of 4 Hz with a descent rate of 1–$2\,\mathrm{m\,s}^{-1}$, yielding 10 to 20 samples for every 5 m of vertical profile. The instrument also logged on recovery, which at a slower ascent rate of 0.3–$0.5\,\mathrm{m\,s}^{-1}$ provided ~ 40 samples per 5 m bin.

Data were filtered by removing points of more than one standard deviation from the un-weighted moving average window ($n = 16$) to yield a statistically significant result. Data were subsequently parsed into 5 m vertical bins for which the mean and standard deviation were calculated. The standard deviation provides an indication of sample stability, and corresponds to $\pm 0.023\,°\mathrm{C}$ for Potential Temperature, ± 0.025 Practical Salinity Unit (PSU) for salinity and ± 1.4 Nephelometric Turbidity Unit (NTU) for the turbidity. Potential Temperature (θ) and Salinity (S) are calculated according to the equations of state of seawater (Fofonoff et al., 2004) and can be used to identify specific water bodies and mixing processes. Turbidity is measured based on back-scattering of light, while the actual reflectivity of turbid water is not only dependent on the concentration of particles but also on the type (lithology and size) of particles which can vary from one fjord to another. To address this potential source of error, we express the turbidity as a percentage of the maximum value recorded for each fjord.

3.2 Water type identification

When plotted in temperature/salinity (θ–S) space, two distinct types of water body can be differentiated. Source water-masses are defined by thick, homogenous layers, in excess of 50 m within the water profile, which share similar temperature and salinity characteristics ($\Delta\theta < 0.2\,°C$ and $\Delta S < 0.2$ PSU). Such water-masses can be identified by dense clustering on θ–S diagrams. Mixed water-masses are defined as a layer within the water column combining two source water-types and are characterised by a line on a θ–S diagram joining the source water types. We define a mixed water-mass when its thickness exceeds 50 m, the gradient $\delta\theta/\delta S$ is constant and that the characteristics of the water shows a substantial difference ($\Delta\theta > 0.5\,°C$ and/or $\Delta S > 0.5$ PSU) between the top and the bottom of the layer.

To track which water body (source or mixed) is driving submarine melt, we calculate the temperature and salinity loss within each water-body that accounts for the melted glacier ice. Given a potential temperature for glacier ice (θ_i) at the front, following Jenkins (1999) and Straneo et al. (2011), we define an effective potential temperature (θ_{eff}) of the corresponding virtual source water type by calculating the energy required to melt a unit weight of that ice as follows:

$$\theta_{eff} = \theta_f - \frac{L_i - C_i \cdot (\theta_f - \theta_i)}{Csw} \tag{1}$$

where θ_f is the pressure corrected melting point of ice; L_i ($337\,kJ\,kg^{-1}$) is the latent heat of fusion; C_i ($2.1\,kJ\,kg^{-1}\,K^{-1}$) the specific heat capacity of ice and C_{sw}($3.9\,kJ\,kg^{-1}\,K^{-1}$) the specific heat capacity of seawater. The resultant mixed water mass will fall along a line between the warm water body driving the subaqueous melt and the virtual source water (θ_{eff}; $S = 0$) in the θ–S diagram. The strength of the melting is depending on temperature difference but also on the dynamic of the water at the interface.

3.3 Interpolation of oceanic measurements

The spatial distribution of temperature, turbidity and salinity were interpolated across and along RF and SF using a triangle-based cubic method. The cross-profile was interpolated immediately adjacent to each ice front ($\sim 200\,\mathrm{m}$) and the long-profile section tracks the mid-point of each fjord. Fjord bathymetry was interpolated from the CTD cast logs.

3.4 Runoff discharge estimation

In addition to synoptic meteorological conditions, glacier surface runoff discharge is dependent upon the ablation area, its elevation-area distribution (i.e., the hypsometry) and the seasonal distribution of snow/ice. Runoff also varies greatly inter- and intra-seasonally depending on the weather each summer. Monthly averaged values of melt over each glacier's ablation area and hence runoff discharge, were estimated following Box (2013), (Table 3). This model uses a monthly estimation of the melt rate using a positive degree-day approach (Box, 2013). The results were then integrated over the catchment area of each glacier using the (Bamber and Aspinall, 2013) elevation and land/ice/sea mask data. The 1 km DEM/mask did not adequately classify the lowest $\sim 400\,\mathrm{m}$ of elevation of RG and SG. For these elevations, the melt is extrapolated using an interpolated fit of melt with elevation that closely follows a linear trend.

3.5 Time lapse imagery

Oblique images of the fronts of SG and RG have been extracted from time-lapse cameras installed on the North and South flanks of each glacier, respectively (Fig. 1; extreme ice survey). The pictures span the period of the surveys. The approximate positions of the fronts have been digitalised for the summer 2009 and 2010 as well as for each winter preceding them (i.e. 2008/2009 and 2009/2010).

4 Results

4.1 Water-bodies analysis

Compiled θ–S plots yield three source water-masses and three mixed water masses within both RF and SF (Fig. 2 and Table 2). All identified water bodies were observed within 200 m of the respective glacier calving margin and are assumed to represent water in direct contact with the submerged ice front.

Source waters:

1. SPMW is characterised by waters that average $S = 34.8 \pm 0.1$ PSU and $\theta = 2.8 \pm 0.2\,°C$ and ranges in depth from 400 m to the fjord bottom (~ 800–1000 m). No significant spatial and interannual variability of the SPMW was observed in any of the surveys, although a sinking (~ 50 m) of the upper limit of the SPMW (characterised by the depth at which the maximum temperature of SPMW is found) is observed in 2010 at both SF and RF.

2. Brine-enriched water (BEW) is constrained by summer warming of the fjord surface to a cold core between 50 to 200 m depth, with a minimum temperature $\theta \sim 0\,°C$ (at ~ 150 m depth) and S ranging between 33.7 and 34.3 PSU. However BEW was only clearly observed at SF in 2010 and only a remnant was visible at SF in 2009 for the most distal (i.e. away from the glacier front) cast (i.e. ~ 10 km from the ice front). BEW was not observed at RF during either survey.

3. Unmixed, glacier runoff discharge (GRW) has not been directly measured during our surveys. This is due to strong mixing near the outlet of the GRW at depth (Xu et al., 2013, 2012) and obvious safety issues in term of providing measurement so near the ice front. Nevertheless, presence of GRW discharge can be identified, even when mixed, by high turbidity water jets that are usually located in the upper part of the water column. Occasionally, at SF, a layer of intense turbidity was also observed just above the seabed. In the absence of any rainfall during either sur-

vey, it is assumed that any variations in the discharge of GRW are predominantly driven by variations in surface melting of the glaciers. The modelled melt in August 2009 and 2010 is roughly the same for both glaciers, with a bulk discharge ranging from ~ 1.0 to $\sim 2.0 \times 10^3 \, \text{m}^3 \, \text{s}^{-1}$. However, due to the difference in ablation area, the bulk runoff capacity of SG is $\sim 35\%$ greater than of RG. Record summer temperatures and melt throughout summer 2010 (As et al., 2012) increased the runoff discharge at both RG and SG by $\sim 30\%$ compared to 2009, and hence the estimated meltwater discharge at SG during summer 2009 was almost identical to that of RG during the warmer 2010 melt-season (Table 3).

Mixed water-masses:

1. Surface Water (SW) is extremely spatially variable. During our surveys, over the course of the melt season, SW ranges in temperature from 0 to 10 °C and in salinity from 28 to 33 PSU. We define the limit of the SW by a density of $\sigma_\theta <$ 26.5 kg m^{-3} as it is usually above this density layer that most of the variability appears. Due to the 5 m bin averaging method used in this study, only limited data are available for this ~ 15 m layer. We therefore do not study its interaction with the glacier front in detail. However the pycnocline at the lower interface of the SW was observed to act as a barrier to all upwelling waters, constraining them below the SW.

2. Melt water (MW) is observed above the SPMW and below the BEW (if present in the fjord) and the SW. It starts to appear approximately 150–250 m above the maximum fjord depth (Fig. 2). It has been observed at depths as shallow as 15 m at RF in 2009 partially mixed with Deep mixed runoff water (DMRW; see below), but usually it is not found above 200 m depth. The observed MW falls along a line of ~ 2.5 °C PSU^{-1}.

3. DMRW was observed during all surveys. It is generally found above 200 m depth and below the SW. However, in 2010 at SF, DMRW was only found between the

SW and ~ 75 m depth. In 2009 for SF and 2010 for RF, DMRW was the only water body present between 200 m and the SW. This water-mass follows a gradient of ~ $0.07\,°C\,PSU^{-1}$.

4.2 Observed processes

4.2.1 Submarine melt

Applying Eq. (1) with a potential ice temperature of $\theta_i (= -10\,°C)$ derived from Jakobshavn Isbrae (Thomas, 2004) and an assumed salinity for ice of $S_{ice} = 0$, PSU for a depth of ~ 500 m (i.e. the base of SG ice front) gives a potential melting point of ice $\theta_f = -0.4\,°C$ and therefore a virtual source water potential temperature $\theta_{eff} = -89.8\,°C$. Using the SPMW ($S = 34.8\,PSU$ and $\theta = 2.8\,°C$), as the main source of submarine melting, we obtain a gradient of $2.4\,°C\,PSU^{-1}$ for meltwater mixing line, which is within the approximation of the gradient (~ $2.5\,°C\,PSU^{-1}$) for the MW (Fig. 3). Note that θ_{eff} is not sensitive to assumed values of θ_i and θ_f.

4.2.2 Runoff mixing

The surveys were conducted over two melt-seasons with very different characteristics: 2010 was record-setting in terms of the absolute temperatures experienced, the extent and magnitude of melt and the overall duration of the melt season (As et al., 2012; Tedesco et al., 2011). In contrast, 2009 temperatures were lower and the melt season shorter. When compared with average climatic conditions experienced in Greenland from 2000–2010, 2009 can be considered an average season (As et al., 2012; Tedesco et al., 2011). During the 2010 survey, one dominant turbid plume was observed at the front of SG. The plume was located in the southern embayment of the glacier front, with a diameter of ~ 1 km. Observation and analysis of time-lapse photography indicate that the plume was active as early as June through the duration of the summer until the end of August coincident with surface melt water and runoff generation. Horizontal surface

outflow from the plume attained speeds up to $\sim 1.5\,\mathrm{m\,s^{-1}}$, sufficient to force brash-ice or mélange out from the embayment. A distinct boundary was observed at the outer limit of the plume, visible by a marked change in water turbidity (Fig. 8). Once the upwelling water loses vertical momentum (i.e. when it reaches the surface or when there is no vertical momentum left), the DMRW sinks back to a depth at which it finds its hydrostatic equilibrium. In most cases, the outflow of DMRW is observed beneath the pycnocline of the SW ($\sim 15\,\mathrm{m}$) at depths ranging from 50–100 m (Fig. 4). At RG, no surface plumes were observed at the glacier front in 2009 and 2010, even when direct observation of the sea surface near the front was possible due to the absence of brash. However, turbid water was observed flowing away from the ice front in concentrated subsurface jets located along both the north and south sides of the fjord. The strongest jet was measured at 15 m depth, just beneath the pycnocline on the north side of the fjord (Fig. 5).

GRW mixing was observed at depths above 200 m in almost all surveys ($\sim 75\,\mathrm{m}$ depth for SF in 2010). Using this depth to define the second apex of the GRW mixing line gives a gradient of $\sim 0.05\,^{\circ}\mathrm{C\,PSU^{-1}}$ for RF in 2009 and 2010, and SF in 2009. The exception of SF in 2010 is caused by the presence of the cold BEW between 75–200 m depth (see below). Therefore, the GRW mixing line for SF in 2010 is calculated for a depth of 75 m and follows a gradient of $0.04\,^{\circ}\mathrm{C\,PSU^{-1}}$ (Fig. 3).

4.2.3 Insulating cold water

An additional process which seasonally impacts the ice front, is the insulating effect of the cold and salty BEW layer that forms in winter (Melling et al., 2001) and occasionally persists through much of the summer melt season. For example, cold BEW was clearly observed at $\sim 200\,\mathrm{m}$ away from the front of SG in mid-August 2010. Due to the near-zero potential temperature of this water, no major melting (i.e. presence of MW) occurs where BEW accumulates along the ice front (Figs. 3 and 5). Because BEW is only produced in winter, it is typically replaced by other warmer water-bodies produced in

Spring/Summer (such as DMRW or MW), which have similar densities, resulting in mixing and the loss of the insulation effect of the BEW (Figs. 4 and 5 – Rink 2009/10). At SF in 2009 a remnant of the insulating BEW was present in the most distal cast (> 10 km) but not near the front (∼ 3 km). However because the cold water was no longer in contact with the glacier front the insulation effect on melting will be negligible (Figs. 4 and 5).

5 Discussion

5.1 Ocean-glacier interaction

Comparison of the two summer surveys enables four modes of ocean–glacier interaction to be distinguished at RG and SG: (1) submarine melting and minimal runoff mixing, (2) runoff mixing and removal of BEW, (3) runoff mixing and preservation of BEW, and (4) submarine melting alone.

From the seabed to approximately 200 m depth (bottom layer), only submarine melting (mode 4) was identified in all surveys at both glaciers in both years (Figs. 4 and 5). In contrast, in the upper 15–200 m (upper layer) of the water column, three modes of interaction can be distinguished: submarine melting and minimal runoff mixing (mode 1 – RF, 2009), runoff mixing and removal of BEW (mode 2 – SF, 2009 and RF, 2010), and runoff mixing and preservation of BEW (mode 3 – SF 2010). Given the apparent stability of deep SPMW at both glaciers throughout 2009 and 2010, along with the recurrent winter build-up of BEW in the upper 200 m of the water column related to sea-ice formation, we assume that for the duration of our surveys, natural oceanic variability was not a dominant effect. Partitioning of the modes in each survey suggested that the development of the upper layer, along with the associated mixing processes, was in fact strongly influenced by the GRW discharge. Indeed the modes observed for the upper layer at SF in 2009 are markedly similar to those observed at RF in 2010 when the two surveys had similar estimates of glacier runoff discharge (Table 3). It

follows that variations in the timing and intensity of GRW injected into the fjord from June to September drive the main changes in the upper layer. A general relationship between the processes observed and the bulk estimated GRW discharge can be identified (Fig. 6): (a) Weak discharge ($\lesssim 1.0 \times 10^3 \, \mathrm{m}^3 \, \mathrm{s}^{-1}$) stimulates submarine melting and minimal runoff mixing (mode 1): GRW forced upwelling at the glacier front is subdued. SPMW forced large scale, weak convection, diffusional melting (hereafter called ubiquitous melt) dominates, and seaward outflow of MW occurs from the glacier toe to the base of the insulating BEW. Eventually the seaward flow of MW removes BEW and submarine melting occurs at all depths up to the base of the halocline. (b) Medium discharge ($\sim 1.5 \times 10^3 \, \mathrm{m}^3 \, \mathrm{s}^{-1}$) stimulates runoff mixing and removal of BEW (mode 2): mixing of GRW with SPMW produces DMRW, which rises as a buoyant plume and intensifies local submarine melting (enhanced buoyancy-driven melting). In this case, DMRW typically reaches hydrostatic equilibrium and flows seaward at ~ 50–$150 \, \mathrm{m}$, quickly removing the BEW and exposing much of the ice front to ubiquitous melting. (c) Strong discharge ($\gtrsim 2.0 \times 10^3 \, \mathrm{m}^3 \, \mathrm{s}^{-1}$) stimulates runoff mixing and preservation of BEW (mode 3): strong buoyant upwelling, which has sufficient vertical momentum to reach the fjord surface, rises along the glacier front. The DMRW is still too dense to be stable at the surface and sinks to hydrostatic equilibrium between 50–100 m, above the cold BEW. Although the BEW is displaced across sectors where runoff driven upwelling occurs, it still insulates much of the remaining ice front and constrains MW to below 200 m depth. Hence, we argue that the variation of GRW significantly affects the summer mode of glacier–ocean interaction along with the associated fjord circulation patterns in the upper water column (0–200 m depth). However, deeper in the water column (> 200 m depth), both glaciers are exclusively affected by submarine melting from persistent interaction with SPMW (mode 4), very likely throughout the year including winter. Hence, at RG where the ice front is up to 750 m deep, only $\sim 75\%$ of the ice face is affected and hence dominated by ubiquitous melting, whilst at SG, where the ice front is 500 m deep, the efficacy of ubiquitous melting is reduced and variability in runoff discharge correspondingly dominates.

5.2 GRW-driven upwelling : spatial spreading and glacier impact

GRW-driven upwelling, producing the DMRW, was commonly associated with enhanced submarine melting through the entrainment of warm water along the ice front (Motyka et al., 2003, 2011; Rignot et al., 2010; Sciascia et al., 2013; Sole et al., 2012) and is assumed to affect the whole glacier front accordingly. Therefore it is usually modelled using a 2-D along fjord section (Salcedo-Castro et al., 2011; Xu et al., 2012) or using 3-D grid limited to the area containing the plume (Xu et al., 2013) (i.e. the model domain does not reproduce the entire front). However, this process is spatially limited along the ice front, confined to areas directly above the portals/conduits where subglacial GRW exits the glacier front (Fig. 6). Analysis of time-lapse photos of the SG front shows that the surface extent of the plume is restricted within an embayment of up to 1 km across (Fig. 8). Moreover, within the surface plume (visually defined by the contrast in water colour), measured turbidity indicates that the plume of DMRW rises vertically along the front and only spreads horizontally once it reaches the surface before sinking to hydrostatic equilibrium below the pycnocline of the SW (Fig. 7). More likely, the vigorous mixing of ambient water with GRW creates a warmer water mixture (DMRW) than otherwise occurs through dilution by submarine melting alone given equivalent ambient water characteristics. Therefore, in the area where the rising plume is in contact with the glacier front, DMRW has both greater kinetic energy and potential thermal energy to melt the ice face, than MW alone. Once the DMRW attains hydrostatic equilibrium with the ambient water, it will displace the corresponding water layer adjacent to the ice front. The spread of DMRW at its hydrostatic level along the front will produce another source of weak forced convection diffusional melting of smaller magnitude but larger spatial extent than the active plume, as most of the kinetic energy will have been lost (Fig. 6).

The buoyancy and hence the level of hydrostatic equilibrium of the DMRW is dependent on the dilution by the inflow of GRW. Thus, the stronger the runoff discharge, the closer to the surface the seaward outflow is to be found (Xu et al., 2012, 2013).

If seaward outflow of DMRW occurs at depths above ~ 100 m, a layer of cold BEW can remain intact (Fig. 4 – Store 2010), whereas outflow at depths between 100 m and 200 m will flush BEW rapidly away from the ice front, subsequently removing the insulating effect of the cold BEW and increasing the contact area between the warm DMRW/MW and the glacier front for potential melt (Figs. 4 and 5 – Rink 2009/10 and Store 2009).

These results are consistent with the multi-process model proposed for Sermilik Fjord in East Greenland (Sciascia et al., 2013; Straneo et al., 2011; Sutherland and Straneo, 2012), as well as with results from a multi-cellular circulation model of Kangerdlugssuaq Fjord forced by melt runoff, tide and wind stress (Sole et al., 2012). In both fjords, glacier runoff discharge-dependant mixing is assumed to affect the entire water column, whilst this study reveals a two-tier structure due to the variable discharge-dependent mixing modes, which appears to only affect the circulation within the upper (< 200 m) water column.

5.3 Oceanic and bathymetric influence on glacier dynamic

Time-lapse observations of the RG and SG fronts indicate daily changes in the behaviour of the calving front, in agreement with the observations from Ahn and Box (2010) of coherent multi-day glacier velocity trends and relatively abrupt slow down. At RG, mass-loss (i.e. calving and melt combined) is relatively homogeneous across the entire ice front with maximum loss, as expected, along the centre-sector, coincident with the deepest part of the fjord and highest ice flow. The plan-view shape of the calving front is concave with no prominent headlands or embayments. A consequence is a relatively flat (plan-view) front over winter and a concave front during summer (Fig. 9). At SG, frontal mass-loss during both summers is greater on the southern flank (glacier left), within a large embayment where an upwelling plume is visible at the surface associated with notches and two headlands constraining the plume. We suggest that these notches are the result of enhanced localized calving/melting due to GRW mixing undercutting the base of the ice face. During winter, the front develops a convex shape

Ice-ocean interaction at two major west Greenland glaciers

N. Chauché et al.

Title Page

Abstract	Introduction
Conclusions	References
Tables	Figures

Back | Close

Full Screen / Esc

Printer-friendly Version

Interactive Discussion

due to the advance of the headlands and the reduced activity of the upwelling plume. The glacier front returns to a flat, uniform ice front once the headlands calve in spring before the start of the melt season. When comparing the shape of the front in summer 2009 and 2010, we observe a more accentuated concave shape at RG in 2009 than 2010. However, the terminus front at SG is straighter in 2009 and with deeper, plan-view, bays and headlands in 2010.

These results suggest that in addition to the glacier dynamics and subglacial topography, the bathymetry of the fjord (i.e. the shape and depth of the fjord bottom at the glacier terminus, allowing the presence of the warm water near the ice front) governs the type and extent of the melt processes that are occurring at the front, and hence has a considerable impact on the calving behaviour and frontal shape. We hypothesize that in Greenland, deep glaciers (~ 750 m) have ice fronts more strongly influenced by large scale, ubiquitous melting than by localised GRW enhanced buoyant plume, favouring a concave ice front and potential big tabular iceberg. For glaciers with shallower fronts (< 500 m), significant GRW-forced localised enhanced buoyancy-driven melting may be overpowering the large scale, ubiquitous melt yielding a crenulated ice front characterised by large embayments separated by prominent headlands where mechanical calving dominates. This hypothesis explains the evolution of the ice front observed between the 2009 and 2010 seasons. At RG, large scale ubiquitous submarine melt resulting in ablation in the deep mid-sector contributes to its concave shape, which in 2009, was more distinct as submarine melting was the dominant process throughout the water-column. In contrast at SG, enhanced plume upwelling dominates over the large scale, ubiquitous melt, accentuating the process of embayment formation, and the prominence of headlands. Higher GRW discharge in 2010 resulted in deeper excavated (plan-view) embayments and prominent headlands.

TCD

7, 5579–5611, 2013

Ice-ocean interaction at two major west Greenland glaciers

N. Chauché et al.

Title Page

Abstract | Introduction

Conclusions | References

Tables | Figures

◄ | ►

◄ | ►

Back | Close

Full Screen / Esc

Printer-friendly Version

Interactive Discussion

6   Conclusions

Our 2009 and 2010 surveys reveal that warm and deep sub-polar mode water (SPMW) was present and in direct contact with two fast-flowing outlet glaciers draining the Greenland ice sheet. Contact between the SPMW and the Rink Glacier (RG) and Store Glacier (SG) ice fronts, at depths of 400 m to their base (750 m/500 m respectively) resulted in the production of submarine melt water (MW), which was present at both glaciers in both survey years. We also find evidence of remnant cold brine-enriched water (BEW) from the previous winter, which can insulate part of the glacier front from melting. Glacier runoff water (GRW) mixing at depth with SPMW yields deep mixed runoff water (DMRW).

Observations of the water structure in each fjord over our two summer surveys are in general agreement with the multilayer fjord circulation model recently proposed for other Greenland fjords (Sciascia et al., 2013; Sole et al., 2012; Straneo et al., 2011; Sutherland and Straneo, 2012).

Interannual variability in the interactions observed at each glacier over two contrasting melt-seasons suggests there is a further level of complexity identified in this study. Our results reveal that the rate of GRW injection into the fjord is a key control on the pattern and efficacy of melt processes in the upper layer above 200 m. Although, GRW plays a major role in governing the mode for the upper layer, it does not affect the bottom layer. Hence, at Rink (750 m deep), where just the top ∼ 25 % of the ice front is affected by variations in GRW, ubiquitous melting dominates and the glacier front evolves to a uniform, concave plan-view profile. In contrast, at Store (500 m deep), enhanced buoyancy-driven melt affects over 40 % of the ice front leading to a crenulated terminus, characterised by embayments separated by major headlands, which are exposed to mechanical calving.

References

Ahn, Y. and Box, J. E.: Glacier velocities from time-lapse photos: technique development and first results from the Extreme Ice Survey (EIS) in Greenland, J. Glaciol., 56, 723–734, 2010.

Bamber, J. L. and Aspinall, W. P.: An expert judgement assessment of future sea level rise from the ice sheets, Nature Climate Change, 3, 424–427, doi:10.1038/nclimate1778, 2013.

Box, J. E.: Greenland ice sheet mass balance reconstruction – Part 2: Surface mass balance (1840–2010), J. Climate, 26, 6974–6989, 2013.

Christoffersen, P., O'Leary, M., and Van Angelen, J.: Partitioning effects from ocean and atmosphere on the calving stability of Kangerdlugssuaq Glacier, East Greenland, Annals, 53, 249–256, 2012.

Fofonoff, N. P., Millard, R. C., SCOR, Data, S. W. G. O. E. O. C., and Standards, U. I. S. I. J. P. O. O. T. A.: Algorithms for computation of fundamental properties of seawater; Unesco technical papers, in: Marine Science, Vol. 44, 1983, 1–58, 2004.

Hanna, E., Huybrechts, P., Steffen, K., Cappelen, J., Huff, R., Shuman, C., Irvine-Fynn, T., Wise, S., and Griffiths, M.: Increased runoff from melt from the Greenland Ice Sheet: a response to global warming, J. Climate, 21, 331–341, doi:10.1175/2007JCLI1964.1, 2008.

Holland, D. M., Thomas, R. H., de Young, B., Ribergaard, M. H., and Lyberth, B.: Acceleration of Jakobshavn Isbrae triggered by warm subsurface ocean waters, Nat. Geosci., 1, 659–664, 2008.

Jenkins, A.: A one-dimensional model of ice shelf-ocean interaction, J. Geophys. Res., 96, 20671–20677, 1991.

Jenkins, A.: The impact of melting ice on ocean waters, J. Phys. Oceanogr., 29, 2370–2381, 1999.

Kjær, K. H., Khan, S. A., Korsgaard, N. J., Wahr, J., Bamber, J. L., Hurkmans, R., van den Broeke, M., Timm, L. H., Kjeldsen, K. K., and Bjørk, A. A.: Aerial photographs reveal late–20th-century dynamic ice loss in northwestern Greenland, Science, 337, 569–573, 2012.

Melling, H., Gratton, Y., and Ingram, G.: Ocean circulation within the North Water Polynya of Baffin Bay, Atmos. Ocean, 39, 301–325, 2001.

Mortensen, J., Lennert, K., Bendtsen, J., and Rysgaard, S.: Heat sources for glacial melt in a subarctic fjord (Godthåbsfjord) in contact with the Greenland Ice Sheet, J. Geophys. Res., 116, C01013, doi:10.1029/2010JC006528, 2011.

Motyka, R. J., Hunter, L., Echelmeyer, K. A., and Connor, C.: Submarine melting at the terminus of a temperate tidewater glacier, LeConte Glacier, Alaska, USA, Ann. Glaciol., 36, 57–65, 2003.

Motyka, R. J., Truffer, M., Fahnestock, M., Mortensen, J., Rysgaard, S., and Howat, I.: Submarine melting of the 1985 Jakobshavn Isbræ floating tongue and the triggering of the current retreat, J. Geophys. Res., 116, F1, doi:10.1029/2009JF001632, 2011.

Mugford, R. and Dowdeswell, J.: Modeling glacial meltwater plume dynamics and sedimentation in highlatitude fjords, J. Geophys. Res., 116, F01023, doi:10.1029/2010JF001735, 2011.

Pfeffer, W. T.: A simple mechanism for irreversible tidewater glacier retreat, J. Geophys. Res., 112, F03S25, doi:10.1029/2006JF000590, 2007.

Rignot, E., Box, J. E., and Hanna, E.: Mass balance of the Greenland ice sheet form 1958 to 2007, Geophys. Res. Lett., 35, L20502, doi:10.1029/2008GL035417, 2008.

Rignot, E., Koppes, M., and Velicogna, I.: Rapid submarine melting of the calving faces of West Greenland glaciers, Nat. Geosci., 3, 187–191, 2010.

Salcedo-Castro, J., Bourgault, D., and deYoung, B.: Circulation induced by subglacial discharge in glacial fjords: results from idealized numerical simulations, Cont. Shelf. Res., 31, 1396–1406, 2011.

Sciascia, R., Straneo, F., Cenedese, C., and Heimbach, P.: Seasonal variability of submarine melt rate and circulation in an East Greenland fjord, J. Geophys. Res.-Oceans, 118, doi:10.1002/jgrc.20142, 2013.

Sole, A. J., Payne, A. J., Nienow, P. W., Christoffersen, P., Cottier, F. R., and Inall, M. E.: Increased glacier runoff enhances the penetration of warm Atlantic water into a large Greenland fjord, The Cryosphere Discuss., 6, 4861–4896, doi:10.5194/tcd-6-4861-2012, 2012.

Straneo, F., Curry, R., Sutherland, D., Hamilton, G., Cenedese, C., Vaage, K., and Stearns, L.: Impact of ocean stratification on submarine melting of a major Greenland outlet glacier, Nature Preceding, 2011.

Title Page

Abstract | Introduction

Conclusions | References

Tables | Figures

|◀ | ▶|

◀ | ▶

Back | Close

Full Screen / Esc

Printer-friendly Version

Interactive Discussion

Straneo, F., Hamilton, G. S., Sutherland, D. A., Stearns, L. A., Davidson, F., Hammill, M. O., Stenson, G. B., and Rosing-Asvid, A.: Rapid circulation of warm subtropical waters in a major glacial fjord in East Greenland, Nat. Geosci., 3, 182–186, 2010.

Sutherland, D. A. and Straneo, F.: Estimating ocean heat transports and submarine melt rates in Sermilik Fjord, Greenland, using lowered acoustic Doppler current profiler (LADCP) velocity profiles, Ann. Glaciol., 53, 50–58, 2012.

Straneo, F., Sutherland, D. A., Holland, D. M., Gladish, C., Hamilton, G. S., Johnson, H. L., Rignot, E., Xu, Y., and Koppes, M.: Characteristics of ocean waters reaching Greenland's glaciers, Ann. Glaciol., 53, 202–210, 2012.

Tedesco, M., Fettweis, X., Van den Broeke, M., Van De Wal, R., Smeets, C., van de Berg, W. J., Serreze, M., and Box, J.: The role of albedo and accumulation in the 2010 melting record in Greenland, Environ. Res. Lett., 6, 014005, doi:10.1088/1748-9326/6/1/014005, 2011.

Thomas, R. H.: Force-perturbation analysis of recent thinning and acceleration of Jakobshavn Isbrae, Greenland, J. Glaciol., 50, 57–66, 2004.

van As, D., Hubbard, A. L., Hasholt, B., Mikkelsen, A. B., van den Broeke, M. R., and Fausto, R. S.: Large surface meltwater discharge from the Kangerlussuaq sector of the Greenland ice sheet during the record-warm year 2010 explained by detailed energy balance observations, The Cryosphere, 6, 199–209, doi:10.5194/tc-6-199-2012, 2012.

Weidick, A. and Bennike, O.: Quaternary glaciation history and glaciology of Jakobshavn Isbræ and the Disko Bugt region, West Greenland: a review, 2007.

Xu, Y., Rignot, E., Menemenlis, D., and Koppes, M.: Numerical experiments on subaqueous melting of Greenland tidewater glaciers in response to ocean warming and enhanced subglacial discharge, Ann. Glaciol., 53, 2012.

Xu, Y., Rignot, E., Fenty, I., and Menemenlis, D.: Subaqueous melting of Store Glacier, West Greenland from threedimensional, highresolution numerical modeling and ocean observations, Geophys. Res. Lett., 2013.

Ice-ocean interaction at two major west Greenland glaciers

N. Chauché et al.

Title Page

Abstract | Introduction

Conclusions | References

Tables | Figures

◀ | ▶

◀ | ▶

Back | Close

Full Screen / Esc

Printer-friendly Version

Interactive Discussion

Table 1. Conductivity-Temperature-Depth (CTD) sensor specifications, MIDAS Valeport 2000.

Sensor	Pressure	Conductivity	Temperature	Turbidity
Type	Strain gauge	Valeport inductive coils	Fast response Platinium Thermometer	Seapoint
Accuracy	0.2 Bar	0.01 mS cm^{-1}	0.01 °C	15 NTU

Table 2. Characteristics of different source waters and mixed water masses observed in the study region.

| | Source water type | | | Mixed water masses | | |
	SPMW	BEW	GRW	MW	DMRW	SW
$[\theta$ (°C), S(PSU)] or $(\delta\theta$ (°C)/ δS(PSU))	[2.8; 34.8]	[0; 34]	[0; 0]	(2.5)	(0.05)	NA
Origin	Sub polar gyre	Winter sea ice formation	Surficial/basal ice melt	Interaction SPMW + Glacier	Interaction RW + deep water	Surface RW + surface heat flux + sea ice formation/melting + vertical mixing + . . .
Transport	Advected by West Greenland Current	Advection + Local formation	Local formation	Local formation	Local formation	Local formation
Depth range	400 m–bottom	∼ 50–200 m	500 m (Store) 750 m (Rink)	200–400 m	15–200 m or 15–75 m	0–15 m

Title Page

Abstract   Introduction

Conclusions   References

Tables   Figures

◄◄   ►►

◄   ►

Back   Close

Full Screen / Esc

Printer-friendly Version

Interactive Discussion

Table 3. Modes of ice front interaction, for the upper layer (0–200 m), associated with runoff (RW) discharge modeled.

Fjord	Year	Mode (Water resulting)	Aug average RW discharge rate ($10^3 \, \mathrm{m^3 \, s^{-1}}$)
Rink	2009	1 (MW, DMRW)	1.12
	2010	2 (DMRW)	1.50
Store	2009	2 (DMRW)	1.53
	2010	3 (BEW, DMRW)	1.99
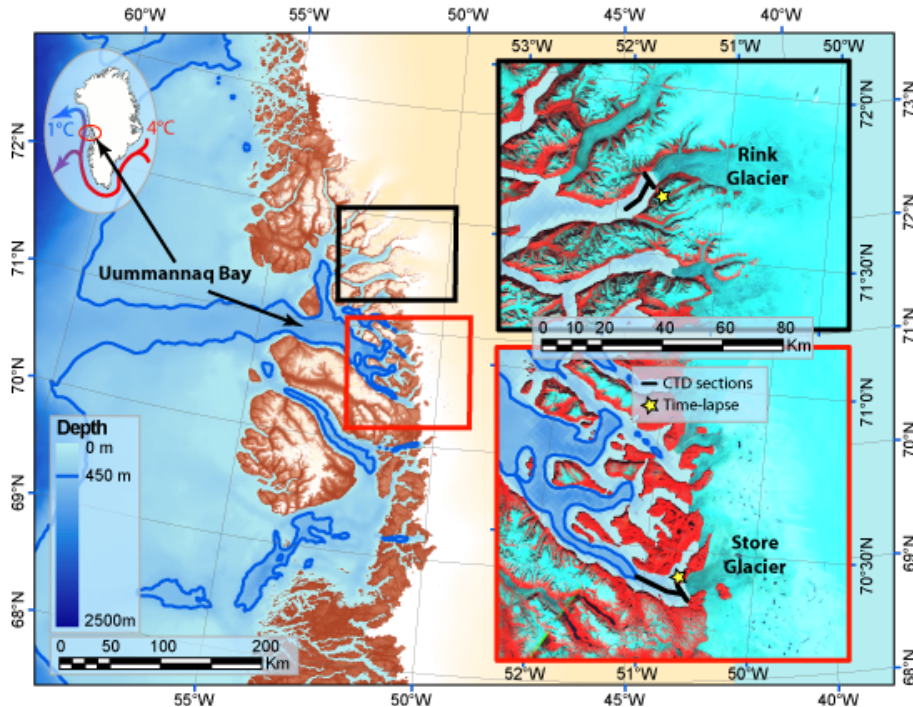
Fig. 1. Map of the study area. The black lines correspond to the CTD sections made across and along the fjords. The 450 m water depth contour line has been highlighted in thick blue to indicate where deep warm SPMW enters the fjord. A false colour Landsat mosaic from August 2010 is used for the inlet maps, superimposed only over land and glaciers. Bathymetry is from International Bathymetry Chart of the Arctic Ocean (IBCAO). Topography (brown shade) and Ice mask (off-white) are taken from Greenland Ice Map Project (GIMP). Note that although the bathymetry appear to be correct for the outer part of the fjord, that of the inner fjords is inaccurate, as depths of up to 800 m and 1100 m have been observed near Store and Rink fronts, respectively.
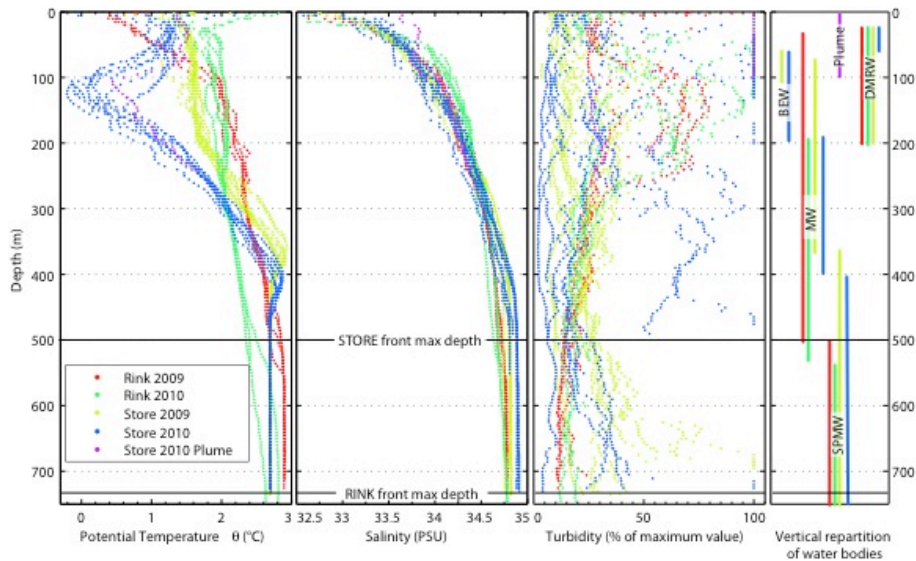
Fig. 2. Potential temperature, salinity and turbidity vs. depth for all the casts of each survey. Each water body identified is shown with a colour corresponding to the surveys during which it was observed. The maximal estimated depths for each glacier are shown by continuous horizontal black lines. The turbidity has been converted to a percentage of the maximum value of each fjord to account for the effect of variable lithology and size of the particles affecting the backscattering light measured with the turbidity sensor. For Store in 2010, the cast which has been done inside the plume, is in purple. It can be seen that the top 100 m of the plume corresponds to maximal turbidity, saltier and relatively warmer water. This is due to the effect of GRW dilution with deep salty and warm SPMW.
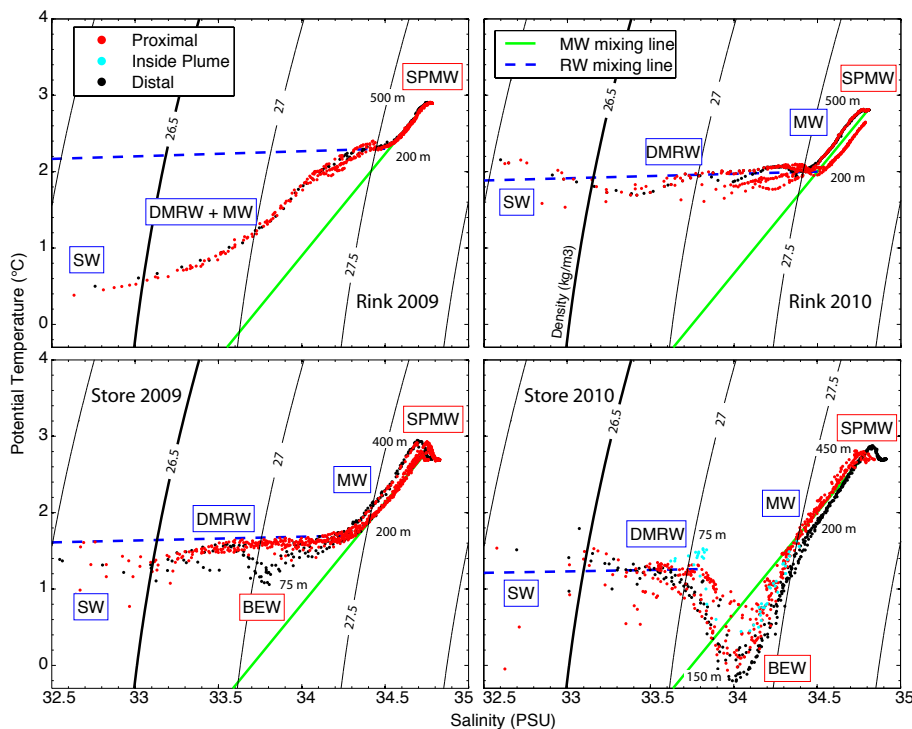
Fig. 3. Temperature–Salinity diagram of the CTD casts in 2009 and 2010 for Rink and Store fjords. The distal (∼ 20–30 km) water masses are in black and the proximal water masses in red (∼ 0.2–1 km). The labels of the source water types are outlined in red and of the mixed water masses in blue. Isopycnals are in black with $\sigma = 26.5$ highlighted in bold to represent the limit of the surface water. Green continuous and blue dashed lines represent mixing due to glacier–ocean interaction processes of submarine melting and run-off mixing, respectively.
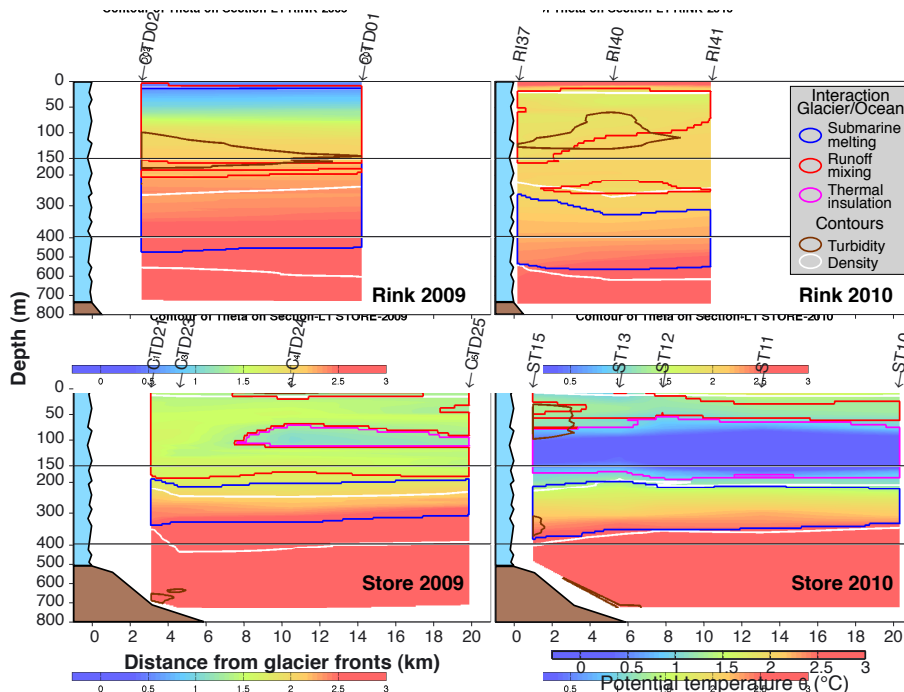
Fig. 4. Potential temperature along fjord section (parallel to the fjord main axe), with the glacier front to the left and the open ocean to the right. The north side of the fjord is on the left and it is looking toward the ice front. The contour lines show waters involved in submarine melting (blue), runoff mixing (red), and thermal insulation (purple). The brown contour shows water > 80 % of the maximum turbidity recorded in the fjord, depicting sediment concentration. The white contour lines correspond to the isopycnic lines of $\sigma = 26.5$; 27 and 27.5. In plain brown is the supposed bottom according to the maximum depth reached by the CTD during the nearest cast.
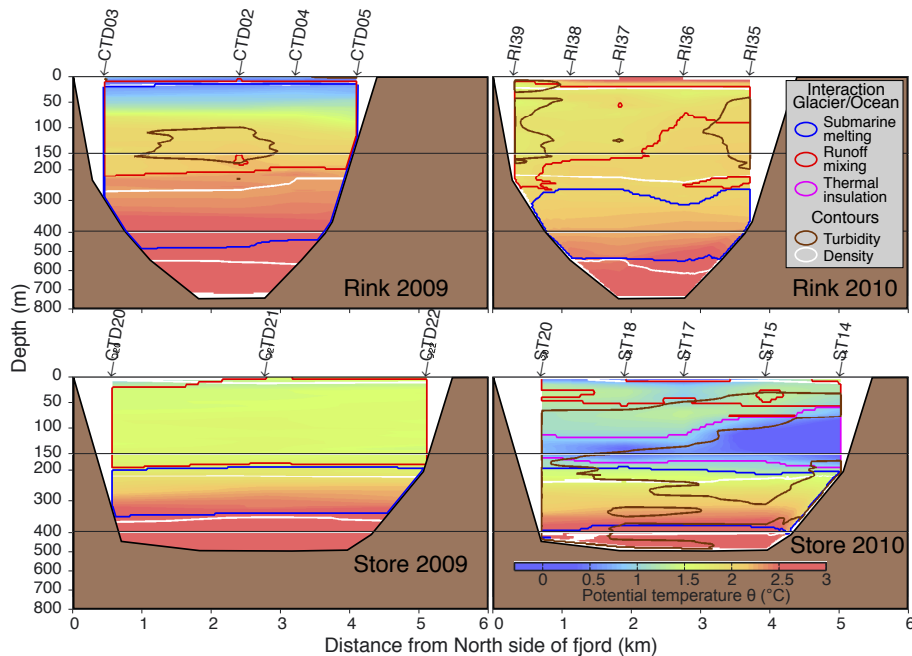
Fig. 5. Same as Fig. 4, but with the across fjord section (parallel to the front at ∼ 200–1000 m distance). The north side of the fjord is on the left and it is looking toward the ice front.

Full Screen / Esc

Printer-friendly Version

Interactive Discussion
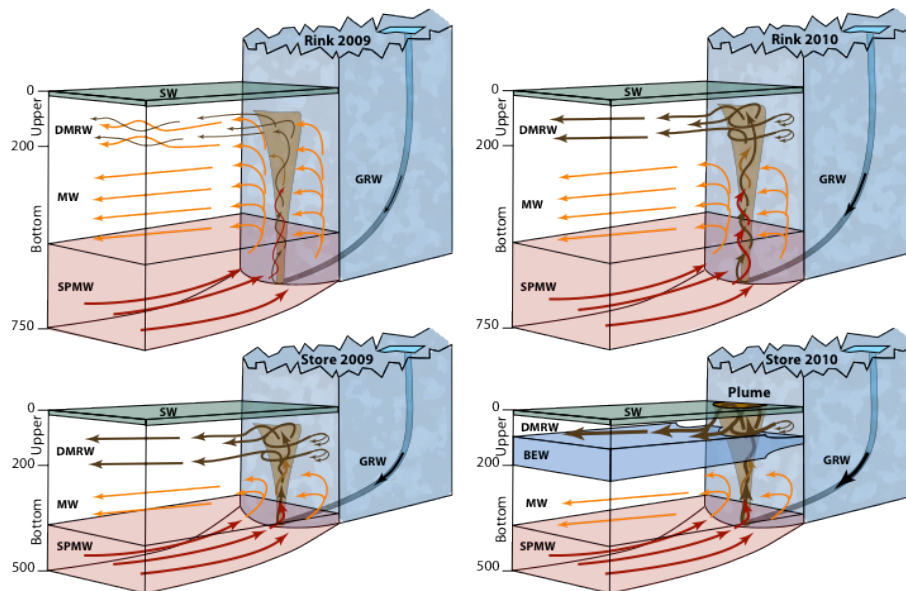
Fig. 6. Schematic interaction processes and circulation at the glacier ice front. The arrows show the different process of interaction with: GRW (black), runoff mixing (brown) submarine melting (orange) and the influx of SPMW (red). The arrow thicknesses represent an estimation of the magnitude of each process. The approximate extent of the turbid plume illustrate that the phenomenon is local and not spread completely across the ice front, although DMRW will be in contact with the glacier at its level of hydrostatic equilibrium. The upper and bottom layers are represented above and below 200 m depth (Sect. 5.1).
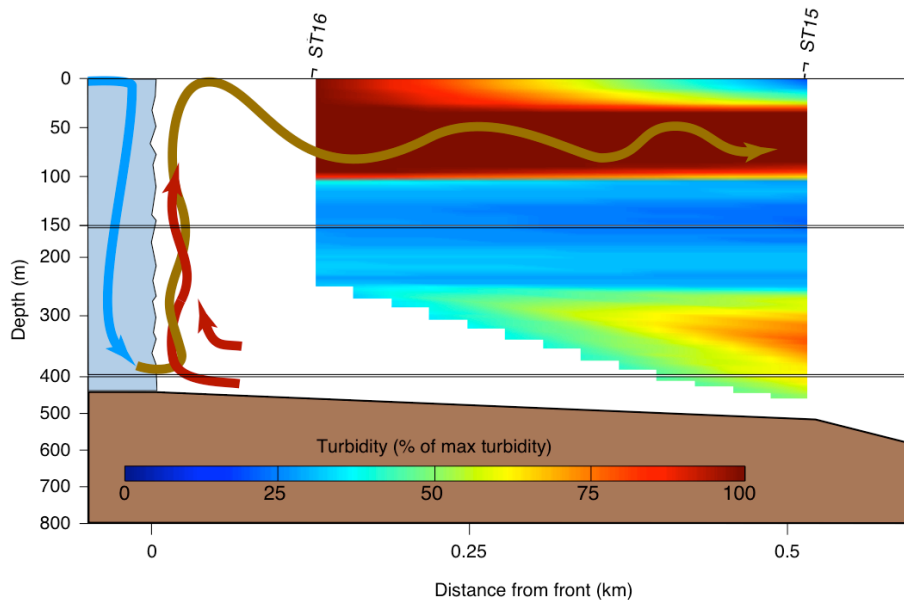
Fig. 7. Turbidity section across the boundary of the surface plume. The turbidity is shown as a percentage of the maximum turbidity recorded. The cast ST15 was done ~ 100 m outside the turbid plume, the surface of the sea was a normal blue colour and no significant surface current was observed. The cast ST16 was done about 100 m inside the surface plume, the colour of the surface was dark brown and a strong turbulent current flowing away from the glacier was observed. ST16 was not lowered to the bottom of the fjord for safety reasons, therefore interpolation below 250 m is not possible. The arrows show a schematics circulation in the plume, with: GRW in blue, SPMW in red and DMRW in brown.

Fig. 8. Picture taken from the southern side of Store Glacier in 2012 (looking north). The red line shows the boundary of the turbid plume observed from June to September and its approximate extent.
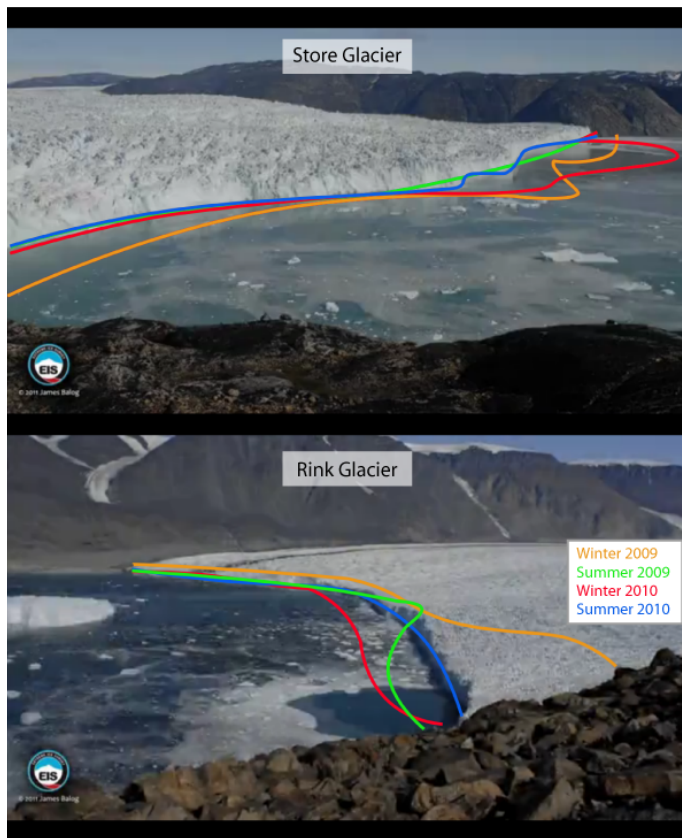
Fig. 9. Extreme Ice Survey (EIS) time-lapse images of Store and Rink glacier termini in August 2010. The general shape and position of each glacier front for the winter preceding each survey and the summer of the survey have been outlined in orange (winter 2009), green (summer 2009), red (winter 2010) and blue (summer 2010).